ROLE OF TECTONIC INDUCED METAMORPHISM ON THE PETROGENESES OF BARITE DEPOSITS HOSTED IN TANAWAL FORMATION, PAKISTAN: PETROGRAPHIC AND GEOCHEMICAL PERSPECTIVES

Saeed Ullah Khan¹, Ijaz Ullah Khan², Shakeel Ahmad³, Ibrar Ul Haq⁴ Saved Abdul Hanan Shah⁵, Salman Khurshid⁶, Imran Ullah⁷, Wajeeh Ullah⁸, Imran Ahmad⁹

^{1,2,3,4,6,7,8,*9}Department of Geology, University of Malakand, Chakdara, 18800, (Pakistan)

⁵Department of Geology, Bacha Khan University, Charsadda, 24420, Pakistan

*9imran_geo@uom.edu.pk

DOI: https://doi.org/10.5281/zenodo.17513520

Keywords

Barite, quantitative analysis, geochemistry, petrography, hydrothermal vein barite.

Article History

Received: 11 September 2025 Accepted: 21 October 2025 Published: 03 November 2025

Copyright @Author Corresponding Author: * Imran Ahmad

Abstract

Barite (barium sulfate, BaSO4) is very important in the oil and gas industry because it is a key ingredient in the oil base mud (OBM) used in the drilling of oil and gas wells. Elemental barium is an additive in optical glass, ceramic glazes, and other products. Based on occurrences, Barite have following four main types: bedded-sedimentary; bedded-volcanic; vein, cavity-fill, and metasomatic and residual. This study considered the formation, occurrence and distribution as well as the utilization and challenges facing in the mining of barite. Extensive fieldwork, selective sampling, petrographic and geochemical analysis were adopted as basic methodology for achieving the objectives of this study. Regional metamorphism in response to local tectonics act as the prominent controlling factors for the formation and paragenesis of barite deposits in the Khanano Dheri Buner area, Pakistan. Genetic relationship of barite deposits hosted in metamorphosed Tanawal Formation located in the lesser Himalayan zone will help in understanding the evolution of other economic mineralization in the region. Field observations, petrographic examination and analytical data interpretation indicate that the formation of barite is closely associated to the tectonic evolution of the region. The deposits are primarily hydrothermal vein deposits, in which barite crystallize from hydrothermal fluids during its migration and circulation in the host formation. This research provides a basic clue for the genesis of barite in high grade metamorphic terrain by hydrothermal mineralization, exhibiting the impact of tectonic evolution, geological history, and stratigraphic framework. Interpretation of geochemical analysis indicate that these barite deposits are epigenetic, formed through the interaction of hydrothermal fluids evolved from solidifying magma in a failed rift system of Permian age. Geochemical analysis reveals significant variations in the concentration of oxides concentrations observed in different samples. We observed inverse relationship between barium oxide (BaO) and sulfur trioxide (SO3), indication an increase in the concentration of BaO triggers decrease in SO₃ concentration, demonstrating geochemically incompatibility. Furthermore, cross plot of CuO vs FeO represents an inverse relationship, exhibiting visible geochemical incompatibility between Cu and Fe. Moreover, the concentration of SrO decrease with decreasing CaO, represents direct relationship and probable geochemical compatibility between Ca and Sr. It has been observed that geochemical compatibility of ZnO and CuO varies significantly, indicating direct relationship as well as similar geochemical compatibility. In most of the analyzed samples the concentration of K_2O is higher as compared to FeO, but exhibiting similar increase, represents a possible geochemical compatibility between K and Fe. Similarly, the concentration of ZnO remained relatively constant in the investigated samples and its interpretation reflects that its relationship in cross plot with SrO is inverse. The concentration of CuO decreases with the increasing amount of CaO, reflecting inverse relationship as well as geochemical incompatibility in the investigated samples.

INTRODUCTION

Barite (BaSO₄) is a high density, chemically stable sulphate mineral with significant industrial and economic importance (Bageri et al., 2020; Arabi et al., 2023). Over 80% of barite produced globally is used in the oil industries as a weighting agent in drilling fluids and other industrial application around the world (USGS <u>2017</u>, <u>2019</u>; Garside, 2020; Afolayan et al., 2021). Other application of barite is in chemical and industrial process such as mineral fillers in various products e.g., paints, plastics, rubber, concrete, brake pads, and clutch plates and barium chemicals, white pigment and paper industry (Ciullo, 1996; Bonel, 2005; Abraham et al., 2021).

Barite deposit is broadly distributed in space and time and occurring in a range of geological environments, including metamorphic (Hanor, 2000), sedimentary (stratiform/stratabound) (Kontak et al., 2006; Deb and Pal, 2015), marine (Monnin and Cividini, 2006), magmatic e.g. metasomatic and residual concentrations, and volcanogenic or bedded-volcanic (Williams Jones et al., 2000) and hydrothermal vein deposits by hydrothermal solutions and cavity-fill types (Margoum et al., 2015; Nadoll et al., 2019; Walter et al., 2019, 2020; Okubo et al., 2020; Muller and Ehle, 2021). Hydrothermal vein-type deposits generally associated with rift valleys, basement-cover unconformities, and large-scale crustal lineaments or fault systems (Walter et al., 2020). Vein-type barite mineralization also formed under a wide range of pressure, temperature, and different fluid sources in a wide geological time domain (Hanor, 2000; Staude et al., 2011, Walter et al., 2020, Zou et al., 2021). Hydrothermal barite form through the precipitation of Ba-bearing fluids along faults and fractures, often in association with basemetal sulfides. In rifted or extensional basins, fault controlled hydrothermal discharge and mixing with seawater or meteoric water can result in generation of high-grade barite lenses or veins. On the other hand, stratiform barite is linked to basin processes, biogeochemical cycling, cold-seep or venting environments and diagenetic concentration of barium in restricted basins (Hanor, Determining which of these genetic pathways operated in the studied area is vital for exploration targeting and assessment of economic potential. Worldwide, the extensional rift basins characterized by a variety of hydrothermal mineralization (Deb and Goodfellow, 2004). In the Indian shield, barite mineralization is known from Palaeo Archaean to the Neoproterozoic age, both stratiform and vein barites are known notably in the Dharwar Craton (Nee lakantam, 1987; Deb et al., 1991; Radhakrishna and Vaidyanadhan, 1997; Muller et al., 2017).

Pakistan hosts important barite occurrences, most notably in the Khuzdar and Las Bela belt of Balochistan (Klinger and Ahmad, 1973; Ahsan and Khan, 1994), with large reserves e.g., Gunga and Duddar has 12 million tons (Ahsan and Khan, 1994), Bankri has 2000 tons, Kundi has 3000 tons reported by Ahmad and Klinger (1963). Smaller occurrences are reported in Nathiagali, Haripur, Havelian, Hazara and Swabi and Buner, Khyber

Pakhtunkhwa (Calkins et al., 1975; Range, 1977 and Malkani, 2000).

The Tanawal Formation in the Buner District, northern Pakistan, is a quartzose, arenaceous to quartzitic unit with a complex Panjal Thrust Himalayan tectono-stratigraphic history. Its brittle structures and quartzitic lithologies create favorable conduits for hydrothermal fluid flow, making it a plausible host for structurally controlled barite mineralization. Tectonics and metamorphism influence both fluid generation and the pathways that focus mineralizing solutions. Barite veins frequently occur at structural intersections, along reactivated faults and within zones of brittle deformation adjacent to metamorphic or magmatic heat sources (Robinson, 1992; Dora et al., 2022; Samaoui et al., 2023). In the tectonically complex Himalayan foreland, due to the collision numerous thrusts and fractures has produced that served as channels for mineralizing fluids. Differences in pressure, temperature, and fluid chemistry along these structures controlled barite precipitation. Hence, evaluating the structural setting, metamorphic influences, and fluid composition is fundamental to understanding the timing and source of barite mineralization in the Khanano Dheri area.

Previous research on barite deposits in Pakistan has primarily focused on the southern and southwestern regions, particularly the Khuzdar-Las Bela belt of Balochistan and the Hazara area of Khyber Pakhtunkhwa, where barite occurs mainly as stratabound or vein-type deposits associated with carbonate and shale sequences (Klinger and Richard, 1973; Ahsan and Mallick, 1999; Ali et al., 2021). These studies have discussed the mineralogical characteristics and industrial potential of barite, but few have addressed the detailed genesis, tectonic controls, and geochemical signatures of barite mineralization in the northern Lesser Himalayan domain. In particular, the barite deposits hosted in the Tanawal Formation of Buner District remain poorly characterized in terms of their structural setting, paragenetic sequence, and fluid evolution. In view of this gap, the present study integrates

In view of this gap, the present study integrates detailed field mapping, structural measurements, petrography, mineralogy, and geochemistry to: (1) characterize textures and paragenesis of barite veins, (2) determine geochemical fingerprints to constrain fluid sources, (3) assess structural and metamorphic controls on mineralization, and (4) evaluate distribution and economic significance for local barite supply. By linking global deposit models to local petrographic and geochemical evidence, this work aims to develop a genetic model for the Khanano Dheri barite occurrences and provide practical insights for future exploration in similar tectono-metamorphic terrains.

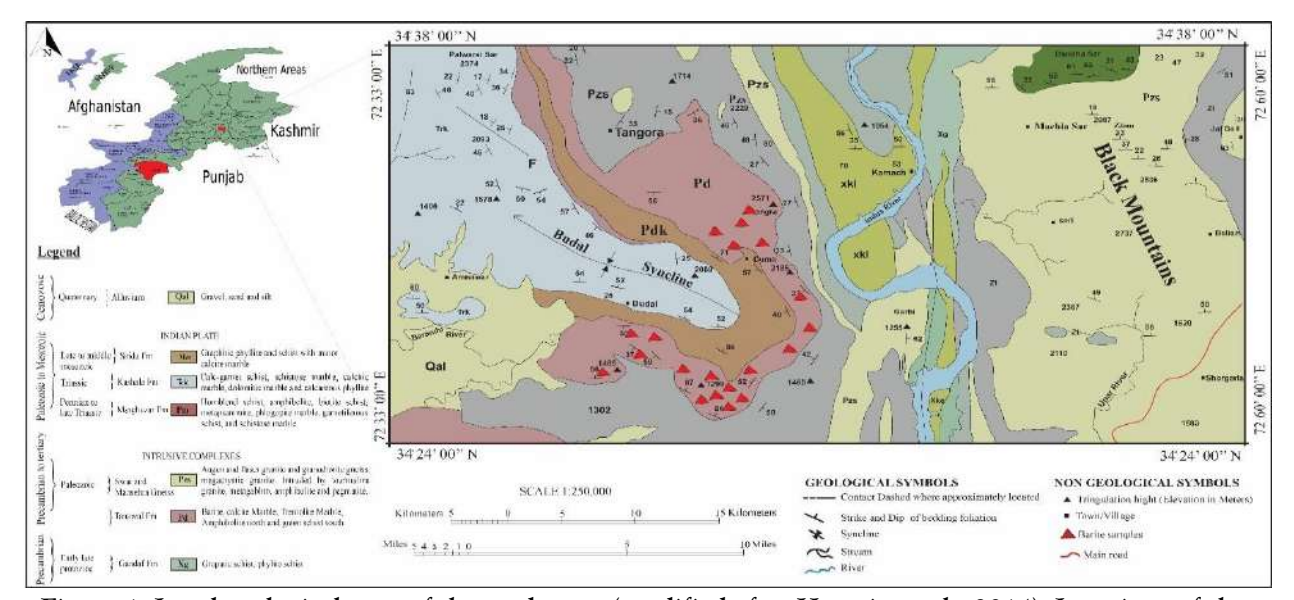


Figure 1. Local geological map of the study area (modified after Hussain et al., 2014). Locations of the collected samples has been marked on the local geological map (red tringles).

2. Study area

The study area is one of the highly tectonic deforms area lies in lesser Himalayas in Northern Pakistan. Barite hydrothermal mineralization is situated in Paleozoic (Precambrian) Tanawal Formation at Longitude 72° 41′ 47″ E and latitude 34° 25′ 46″ N, with elevation of 2 m from sea level, which is the Hazara overlies **Formation** and by overlain unconformable the Kingriali Formation (Figure. 2). In the northwestern Hazara ranges, Barite deposit of the Tanawal Formation 02).

occurs in the hanging wall of the Panjal Thrust (Calkins et al., 1975). Main Geological structural feature observed near the study area is the Nikanai Ghar Fault, which exhibits an east-west (E-W) strike and steep southerly dip. This fault represents a major tectonic discontinuity in the region; however, it describes fault geometry rather than the bedding orientation within the Tanawal Formation itself (University of the Punjab, 20

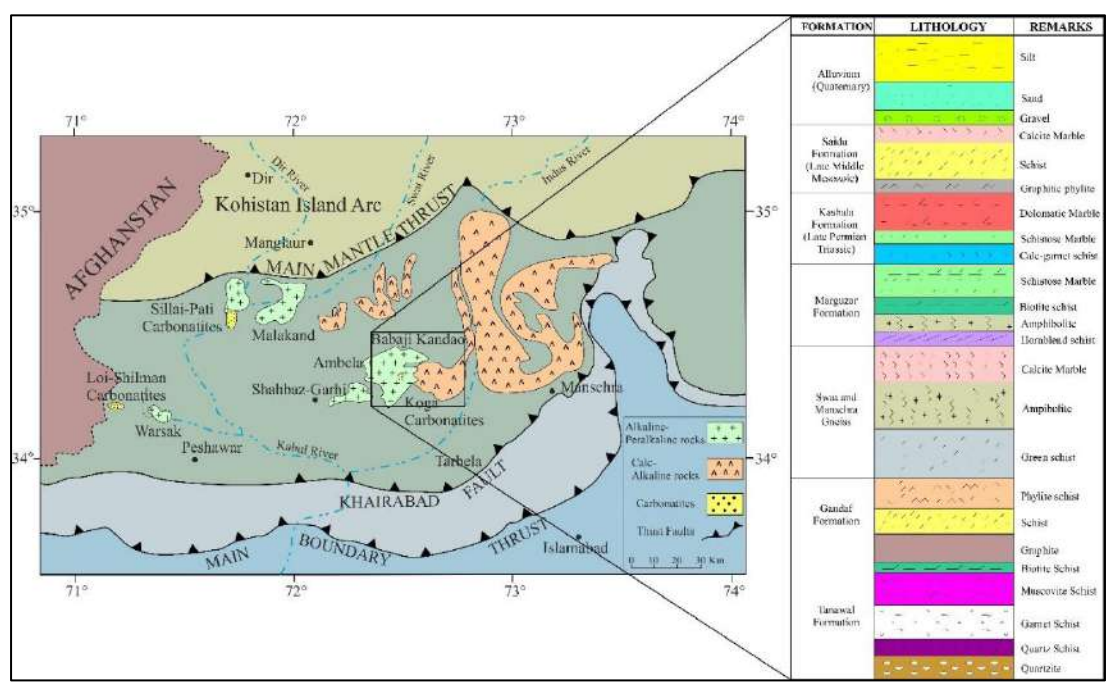


Figure 2. Regional geological map and generalized stratigraphic column of the study area (modified after Ahmad Hussain, Joseph A. DiPietro, Kevin R, Pouge and Irshad Ahmad, 2004).

3. Methodology

The study was initiated with a desk-based review of the regional stratigraphy and tectonic framework. Relevant literature, including Geology of Pakistan (Bender and Raza), Stratigraphy of Pakistan (Shah), Tectonics of Pakistan (Kazmi and Jan), and published research articles, was consulted to establish a geological context and design an effective fieldwork strategy.

Field investigations were conducted mainly through foot traverses across the mapped area. Barite-bearing veins were examined, and structural measurements were recorded. Twenty-five representative samples were collected, from which representative samples were selected for detailed petrographic and geochemical analyses based on their mineralogical and textural characteristics. Hand specimens were first studied in the field, followed by preparation of thin sections at the Department of Geology, Bacha Khan University, Charsadda.

Petrographic examination was carried out under plane polarized and cross polarized light microscope at the National Centre of Excellence in Geology, University of Peshawar and photomicrographs were obtained using an attached digital camera. Observations acquired at magnifications of 5×, 10×, and 20× to identify barite and related gangue

minerals, and to characterize mineralogical connections within hydrothermal veins.

Geochemical analysis of barite was carried out using X-Ray Fluorescence (XRF) spectrometer to evaluate the chemical composition and assess the overall quality. Representative sample for XRF analysis were prepared followed standard procedures: (i) cleaning and washing to eliminate surface contaminants, (ii) pulverizing the samples to approximately 75 μ m using a ball mill, and (iii) drying at temperature of

105 °C until a constant weight was achieved. To enhance the accuracy, the fusion method was applied in which powdered sample were mixed with the lithium tetraborate flux a ratio of 1:10 and heating at temperature of 950-1050 °C to yield homogeneous glass beads. These methods minimize the matrix interferences and particle size effects enabling accurate determination of BaSO₄ concentration.

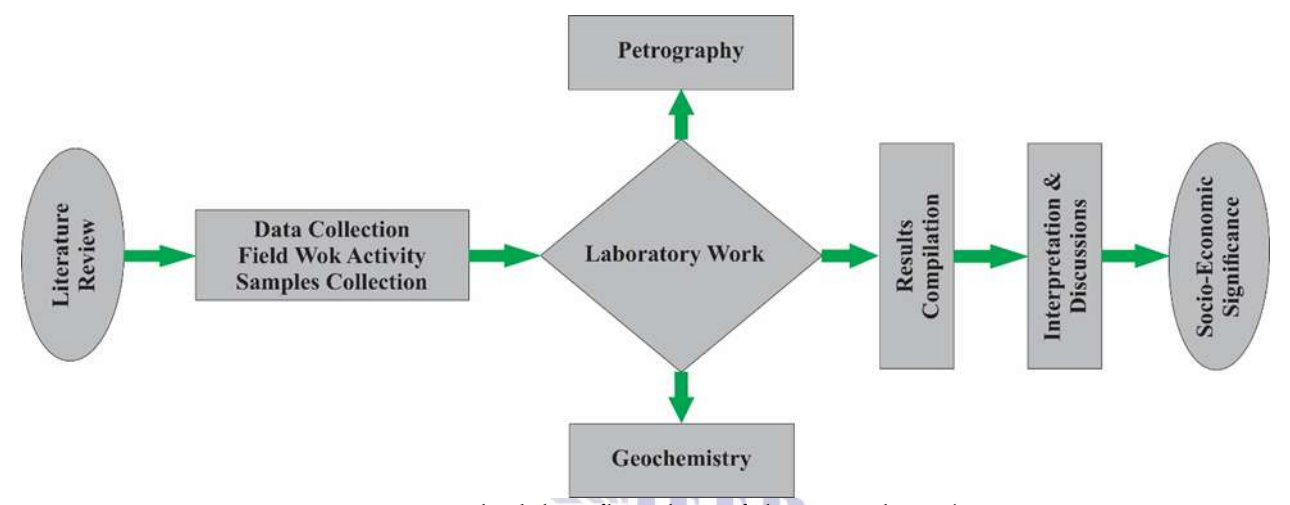


Figure 3. Methodology flow chart of the research work.

4. Results

4.1 Field Observation

Field investigations were carried out at the Khanano Dheri, District Buner, Khyber Pakhtunkhwa. The area is comprised of Kashala, Nikhani Ghar, Tanawal, Saidu Schist and Gandaf Formation. The study focused on the Tanawal Formation, consists mainly of quartos schist, quartzite and schistose conglomerate (Figure. 2). The unit is well exposed in the south and southeastern margin of the Mansehra Granite. Barite deposits were observed in the form of vein (hydrothermal fluid) which is hosted by calcitic and dolomitic marble the Tanawal Formation (Figure. 4A). The barite vein has variable thickness and morphology in different areas. The vein has sharp and well develop contact with the host rock marked by alteration halo or ferruginous staining. Barite vein are typically 1-5 meters thick and 10-50 meters long elongated along strike and dip (Figure. 4A). The color of veins is white to greyish white, and coarse-grained. The studied area

barite is hosted by dolomitic marble and by quartzite locally. In many exposures multiple generations of barite veins were observed. The thick massive units are cut or bordered by smaller, irregular barite-filled stringers and fracture infillings (Figure 4B). These secondary veins have pinch-and-swell geometry and are generally discontinuous, indicating reactivation of the same fracture system at various mineralization phases. Most of the veins are parallel to the bedding or foliation planes of the host marble, while some are discordant, crosscutting the host rock (Figure 4C). Barite mineralization is spatially associated with minor metallic occurrences. Specifically, copper and galena traces were observed along the peripheries and fracture zones adjacent to barite-rich veins (Figures 4D-E). These sulfide minerals occur as small disseminations, streaks, or coatings in the host rock and vein margins, but they are volumetrically minor compare to barite. Overall, the field observation delineates an extensive network of barite veins within the studied area (Tanawal Formation), structurally controlled by faults, joints, and bedding-parallel shear zones. The outcrops are easily recognizable in the field due to the white color and high density of barite compared to the enclosing

rocks. The combination of thick, massive veins and thin fracture-fill barite veins defines the main mode of mineral occurrence in the Khanano Dheri area (Figure 4).

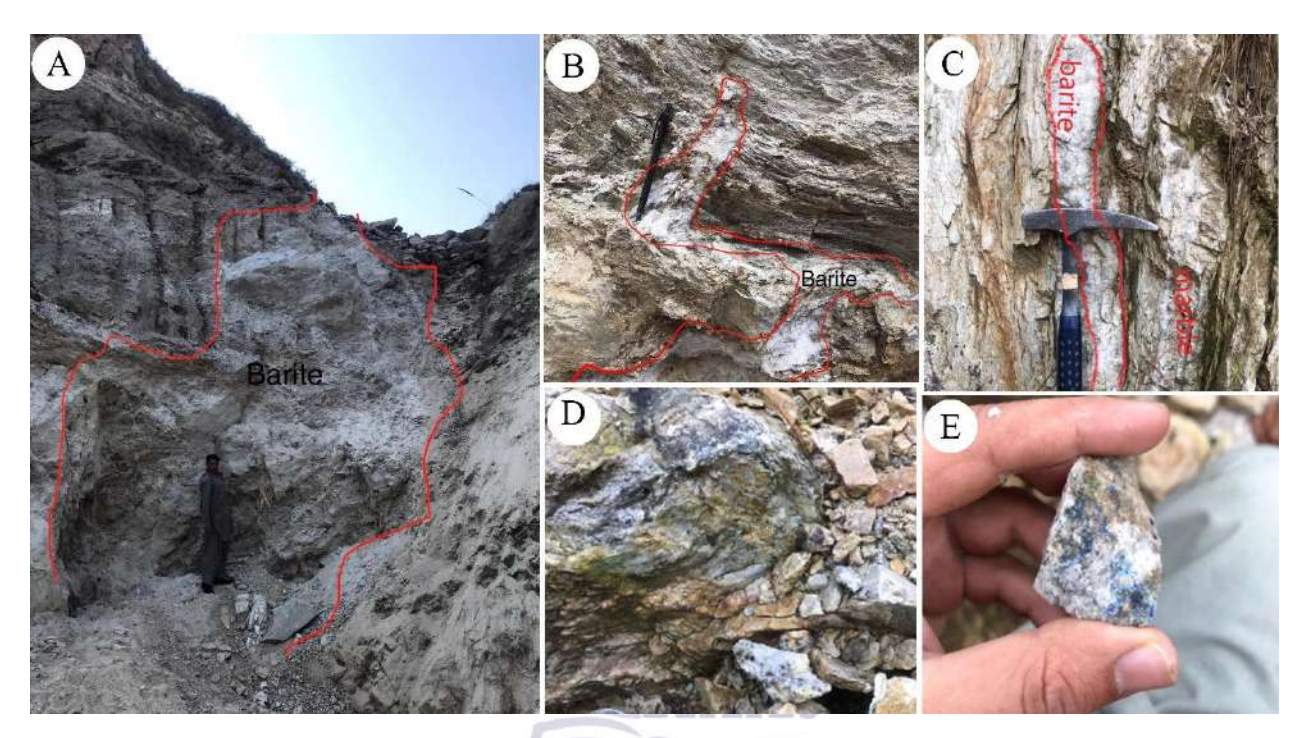


Figure. 4. Field photographs exhibiting prominent features observed during detail outcrop investigations (A) Barite mineralization in a thick vein form in the pre-cambrian Tanawal Formation. Based on cross cutting relationship with the host rock, suggesting its formation in late stages. (B) Numerous amount of small and thin, irregular barite filled veisn wer also observed in the investigated area. (C) most of the investigated veins are bedding parallel and few are in discordant contact with the inherited sedimentary bedding in the host Tanawal Formation. (D-E) Some traces of copper and galena mineralization were also observed along the pheriphery of barite mineralization in specific zone.

4.2 Petrography

The petrographic study of barite samples from the Tanawal Formation reveals a dominant association of barite, quartz, and mica minerals, with minor sulfides and accessory carbonates (Figures 5-7). Barite was identified as coarse grained, moderate relief bladed or tubular texture subhedral to anhedral

crystals (Figures 5C-D). Under plane and cross polarized light, the cleavages are perfect on (001), nearly perfect on (210), and good on (010) with weak pleochroism, high birefringence and rolling extinction. In thin sectional view, barite is marked by red arrows (Figures 5-7). Quartz is observed and identified in thin section, commonly intergrown with barite and appears as medium to coarse grained, undulose extension with straight boundary, high visibility and texture rims. Quartz is marked by sky-blue arrows (Figures 5A-D, 6A-D, 7A-D). Biotite is another mineral which is identified by its moderate relief, greenish to brown color, and it is marked by dark blue color arrows in thin sectional view. Other one mineral which is identified is muscovite mica which has distinguished from others minerals by its flaky texture and it is a shade of green red or brown which is marked by yellow color in thin section. Pyrite is another mineral which is identified (Figure 5A-C) it is cubic in form, high relief opaque in both XPL and PPL and it is marked by white arrow in thin section. Others accessory

mineral include calcite, dolomite, galena, azurite, malachite and siderite is also present in barite thin section.

Barite is frequently represented by large plate like or centimeter-scale tabular crystals or automorphic orthorhombic crystals (Figure 6A-C) of varying sizes due to uniform growth rates. It typically appears as white, pink, or gray masses (Figure 7B). The barite veins of the studied area contained 60-70 vol% barite, ~10-20 vol% quartz, 15-20 vol% biotite and

-1 vol% sulfide minerals in the form of galena, chalcopyrite, and their oxidation minerals (malachite, azurite, iron oxide, and manganese oxide). Due to the remobilization of silicates and sulfides along fractures by hydrothermal fluids, significant network textures have been observed in barite. Microscopically, barite appears as elongated, curved, intertwined, and interlocking long prismatic rods with rolling extinction (Figure 7A-C).

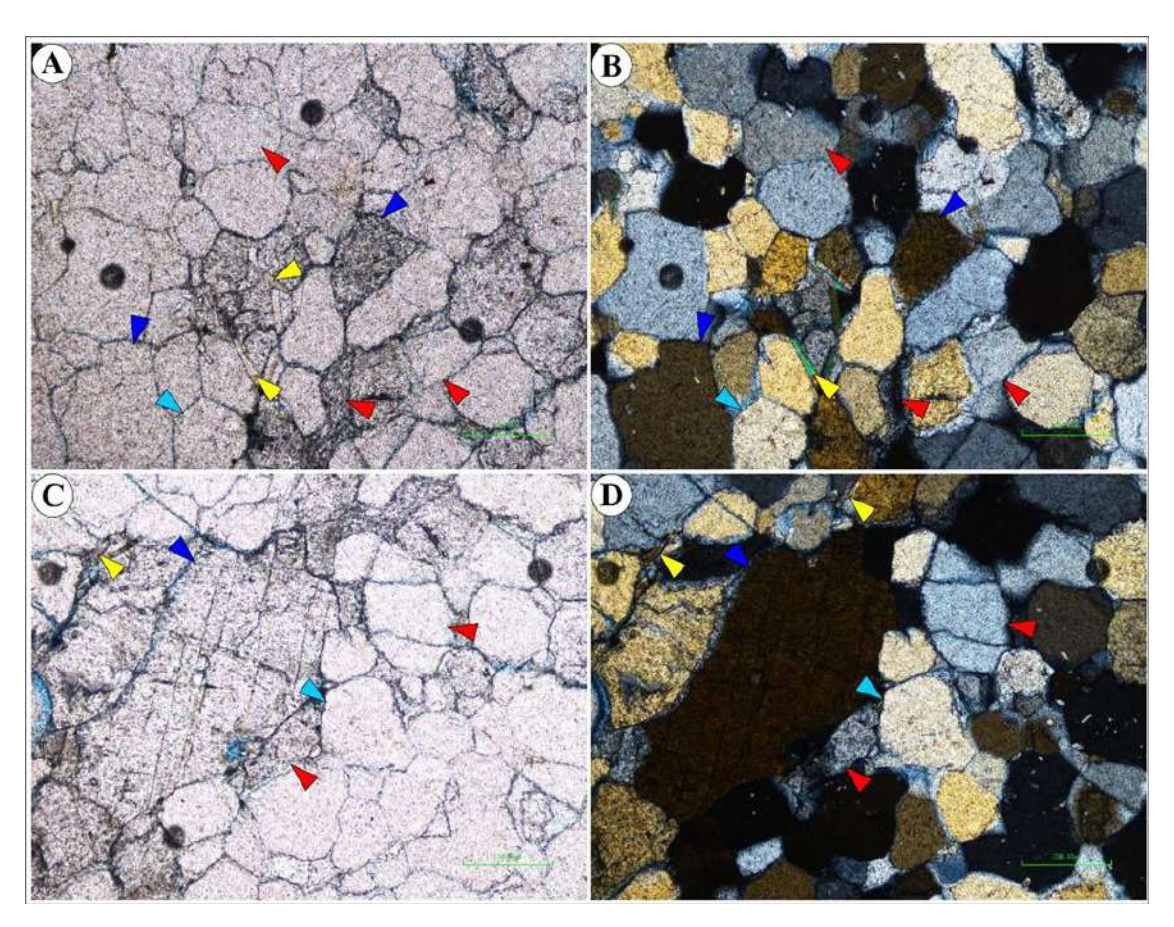


Figure 5. Plain and cross light photomicrographs illustrating textural relationships of barite and associated minerals in the barite vein. (A-B) photomicrographs exhibit anhedral barite grains (red arrows) associated with quartz grains (sky blue arrows). Other associated minerals observed in this association are biotite (dark blue color) and

muscovite (yellow color). (C-D) demonstrates anhedral barite grains (red arrows) associated with quartz grains (sky blue arrows). Very large biotite grain (dark blue color) was observed in close association with quartz and barite grains, while muscovite (yellow color) is present in trace amount.

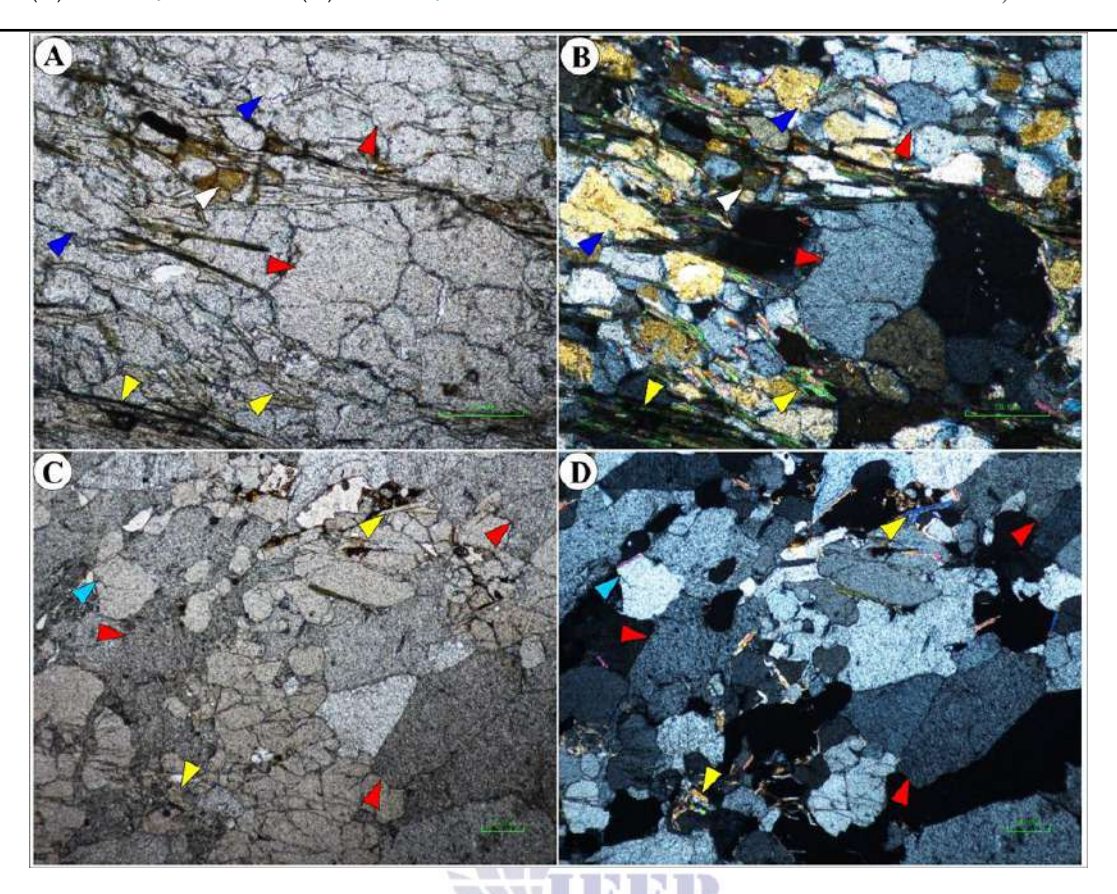


Figure 6. Conventional plain and cross light petrographic observations observed are (A-B) very coarsely crystalline, well developed anhedral barite grains (red arrows) was observed in direct association with medium to coarsely crystalline quartz crystal (sky blue arrows). Trace minerals associated with this setting are biotite (dark blue color) and muscovite

(yellow color). (C-D) demonstrates anhedral barite grains (red arrows) associated with quartz grains (sky blue arrows). Medium grained biotite grain (dark blue color) was observed in close association with quartz and barite grains, while muscovite (yellow color) is present in trace amount.

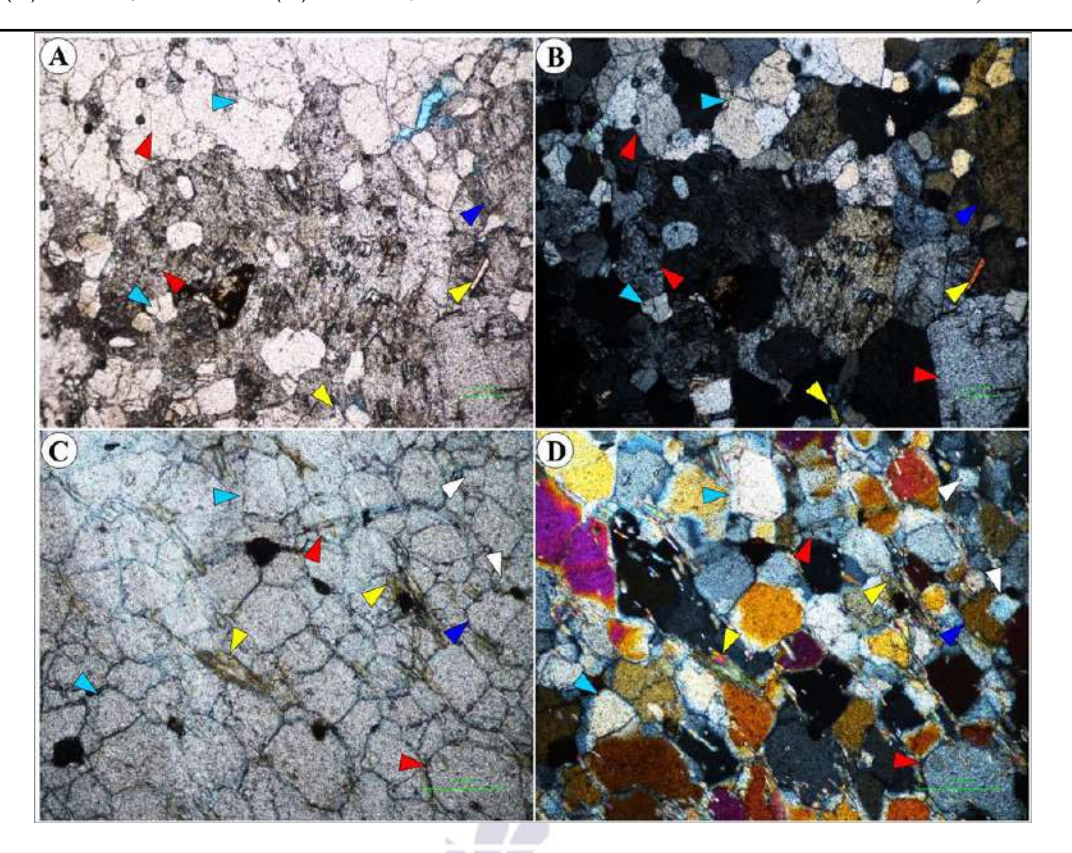


Figure 7. Plain and cross light photomicrographs indicate (A-B) photomicrographs exhibits well developed coarsely crystalline anhedral barite grains (red arrows) associated with coarse quartz crystal (sky blue arrows). Trace minerals associated with this setting are biotite (dark blue color) and muscovite (yellow color). (C-D) demonstrates anhedral barite grains (red arrows) associated with quartz grains (sky blue arrows). Medium grained biotite grain (dark blue color) was observed in close association with quartz and barite grains, while muscovite (yellow color) is present in trace amount.

4.3 Geochemistry

Geochemical studies using XRF on representative rock samples from the Tanawal Formation were employed to determine their elemental composition. XRF is an analytical technique that quantifies various elements within a rock sample. The geochemistry of different oxides was examined using X-ray fluorescence spectroscopic analysis. The different major element and oxides composition present in rock samples are presented in Table 1 and 2. The major element composition of the analysed

samples are given; the specific gravity of the analysed samples ranges from 3.73 (BS-1) to 4.27 (BS-18). The BaSO₄ content of the analyzed samples varies from 75.4 (BS-1) to 94.3 (BS-11). The highest BaSO₄ concentration occurs in sample BS-11 (94.3), followed by BS-18 (93.1), BS-14 (92.8), and BS-13 (90.3), whereas the lowest is recorded in BS-1 (75.4). There is an inverse trend between Silica (SiO₂) and BaSO₄, ranging from 1.56 (BS-11) to 14.55 (BS-1). Whereas calcium carbonate (CaCO₃) content varies from 0.71 (BS-11) to 6.78 (BS-1), indicating local calcite or dolomite contamination. While the Fe₂O₃ content is generally very low, between 0.00-0.21, with slightly elevated values in BS-20 (0.21) and BS-19 (0.19), showing negligible iron substitution in the investigated sample. The oxide composition in the analysed sample is given; the BaO values range from 52.91 (BS-6) to 67.04 (BS-3). The highest BaO concentration in BS-3 (67.04) corresponds to one of the highest BaSO₄ contents, confirming consistent enrichment of barium across the samples. Whereas the lowest BaO is observed in rock sample BS-6 (52.91), which also exhibits relatively elevated SiO₂ and SO₃ contents. CaO values are very low, typically

0.03-0.37, with the maximum in BS-4 (0.37) and the minimum in BS-17 (0.03). The FeO content is negligible (< 0.10), while the maximum value is 0.08 in sample BS-18. The K₂O concentrations are generally low (0.01-1.17), the highest value is 1.17 in BS-20, which may reflect traces of K-bearing silicate

impurities. SO₃ contents range from 31.47 (BS-3) to 46.5 (BS-16). SrO varies from 0.06 (BS-19) to 1.09 (BS-5), with most samples showing 0.3-1.0, indicating limited strontium substitution for barium in the barite lattice.

Table 1. Major oxides detected during qualitative analysis of the representative barite samples collected from Precambrian Tanawal Formation, using X-Ray Florescence Spectrometry.

Sample	Specific gravity	BaSO4	SiO2	CaCO3	Fe2O3
BS-1	3.73	75.4	14.55	6.78	0
BS-2	3.95	83.6	9.02	3.23	0
BS-3	4.13	88.2	5.65	2.02	0.03
BS-4	4.07	85.8	7.41	2.72	0.02
BS-5	4.11	86.11	5.19	4.00	0
BS-6	3.91	82.3	4.00	3.91	0
BS-7	3.76	81.2	4.32	5.72	0.01
BS-8	4.04	85.1	2.67	2.98	0
BS-9	4.16	88.50	5.12	1.94	0.03
BS-10	4.09	86.23	5.33	4.45	0.04
BS-11	4.22	93.45	1.56	0.77	0.02
BS-12	3.98	84.47	9.53	2.01	0.05
BS-13	4.14	90.30	4.25	2.31	0.03
BS-14	4.18	92.78	3.09	0.23	0.04
BS-15	3.78	81.4	12.44	2.30	0.01
BS-16	3.97	85.14	4.67	3.00	0.03
BS-17	4.24	92.78 for Excellence in	Ecocation 1.38 acts	1.4	0.05
BS-18	4.27	93.10	1.11	1.52	0.08
BS-19	4.17	89.1	4.08	2.65	0.19
BS-20	3.99	87.19	7.60	1.22	0.21

Table 2. Minor oxides detected during qualitative analysis of the representative samples using X-Ray Florescence Spectrometry.

Sample	BaO	CaO	FeO	K ₂ O	SO ₃	SrO
BS-1	64.59	0.33	0	0	34.5	1
BS-2	57.89	0.25	0	0.03	39.63	1.07
BS-3	67.04	0.29	0.03	0	31.47	1.02
B S-4	62.33	0.37	0.02	0.04	35.07	1.09
BS-5	61.51	0.31	0	0.01	36.13	1.09
BS-6	59.43	0.23	0	0.441	38.1	0.41
BS-7	52.91	0.27	0.01	0.561	43.75	0.39
BS-8	58.12	0.25	0	0.531	40.01	0.40
BS-9	53.75	0.33	0.03	0.339	45.03	0.45
BS-10	56.19	0.28	0.04	0.435	37.61	0.37
BS-11	63.46	0.26	0.02	0.48	36.3	0.31
BS-12	59.50	0.29	0.05	0.45	38.5	0.41
BS-13	55.11	0.27	0.03	0.46	43.7	0.39

BS-14	62.79	0.28	0.04	0.49	35.9	0.4
BS-15	55.24	0.05	0.01	0.018	44.7	0.6
BS-16	53.11	0.07	0.03	0.014	46.5	0.9
BS-17	54.66	0.09	0.05	0.019	44.1	0.8
BS-18	57.74	0.30	0.08	0.39	42.3	0.2
BS-19	56.74	0	0.19	1.13	41.5	0.06
BS-20	60.11	0.03	0.21	1.17	37.7	0.09

4. Interpretation of Geochemistry

To better understand the compositional relationships among the analyzed oxides and their genetic implications, a detailed geochemical compatibility analysis was conducted. These compatibility trends have been outlined in the following subsections, focusing on the major elemental associations between mineral stages and oxides and trace element correlations.

4.1 Major Elemental Compatibility among Mineral Phases

4.1.1 Geochemical Compatibility of BaSO₄ and SiO₂

Variable concentrations of BaSO₄ determined in the examined rock samples are from 93.45% to 75.4%, whereas the concentration of SiO2 contents were also observed, i.e., from 14.55% to 1.11% (Table 1). The detected BaSO₄ and SiO₂ were then used to determine their geochemical compatibility in the inspected rock samples. For relative trend a cross plot between BaSO₄ and SiO₂ has been established (Figure 8A). The geochemical relationship of BaSO₄ and SiO2 shows a that barite is dominance over silica content, with BaSO₄ ranges from 75.4% (BS-1) to 93.45% (BS-11), whereas SiO₂ content is low (below 10%). Samples having higher SiO₂ content, i.e., BS-1 (14.55%) and BS-15 (12.44%), shows reduced BaSO₄ contents, demonstrating localized siliciclastic or hydrothermal input. In contrast, the most bariteenriched samples, including BS-11 (93.45% BaSO₄, 1.56% SiO₂) and BS-18 (93.1% BaSO₄, 1.11% SiO₂), demonstrate near-complete exclusion of silica. The cross plot of these oxides indicates an inverse relationship between the concentrations of BaSO₄ and SiO₂ (Figure 8A). This inverse trend shows that BaSO₄ and SiO₂, are geochemical incompatible due to barite rich environments which suppressing silica accumulation. Overall, the distribution shows robust

lithological control, where samples rich with BaSO₄ content represent primary ore zones, while the high content of SiO₂ shows minor external contributions.

4.1.2 Geochemical Compatibility of BaSO₄ and CaCO₃

Oxides with variable concentrations were detected in the investigated rock samples, which include BaSO₄ from 75.4% (BS-1) to 93.45% (BS-11) and CaCO₃ (0.23% to 6.78%), respectively. The relative distribution of BaSO₄ and CaCO₃ content shows that barite is dominant in the studied samples. Samples such as BS-1 (BaSO₄ = 75.4%, CaCO₃ = 6.78%) and BS-7 (BaSO₄ = 81.2%, CaCO₃ = 5.72%) record slightly elevated CaCO3, but this is always associated with reduced BaSO₄ (Figure 8B). Conversely, the most barite-enriched samples, including BS-11 (93.45% BaSO₄, 0.77% CaCO₃) and BS-14 (92.78% BaSO₄, 0.23% CaCO₃), demonstrate near-complete exclusion of carbonate phases. From the above oxide values a reverse trend has been established between BaSO4 and CaCO3 indicates these two oxides is not geochemically compatible, because barite mineralization taking place in unfavorable environments for substantial carbonate enrichment. This distribution highlights lithological control, where zones rich with BaSO₄ represent primary barite ore, while minor CaCO3 enrichments reflect restricted carbonate contribution.

4.1.3 Geochemical Compatibility of CaCO₃ and SiO₂

Variable concentrations of calcium carbonate and silica were observed in the investigated rock samples, a cross plot of CaCO₃ vs SiO₂ has been established (Figure 5D) which demonstrations their geochemical compatibility. The results shows that SiO₂ content is

relatively higher is several samples, i.e., 15.2% in BS-1, 10.1% in BS-12, and nearly 13.5% in BS-15, whereas CaCO3 content is much lower in these samples, fluctuating around 2.3-3.1%. Conversely, samples such as BS-5, BS-6, and BS-7 shows more balanced and overall lower concentrations of both oxides, with SiO₂ values averaging about 5.4-6.2% and CaCO₃ between 3.2-4.5% (Figure 8C). The given cross plot exhibits an inverse relationship between CaCO3 and SiO2, where samples having more content of SiO2 shows lower concentration of CaCO₃ and vice versa (Figure 8C). The behavior of geochemical concentration of these oxides can be explained by their different lithological affinities. The samples enriched with SiO₂ are most likely in association with siliceous material or hydrothermal silica input, which tends to dilute or replace carbonate stages throughout deposition or later diagenesis. This is evident in the investigated sample i.e., BS-1 and BS-15, where high silica contents correspond to very low content of carbonate, suggesting that the process of siliciclastic or hydrothermal was dominant. In contrast, relatively higher concentration of CaCO₃, such as in BS-6 (4.7%) and BS-7 (4.3%), occur where SiO₂ is reduced, indicating that the environment was dominated by carbonate, probably connected to primary carbonate deposition or local carbonate replacement zones.

4.1.4 Geochemical Compatibility of CaCO₃ and Fe₂O₃

CaCO₃ values determined in representative rock samples are ranging from 0.23% to 6.78% whereas Fe₂O₃ values are from 0% to 0.21%. In order to understand the geochemical relationship between CaCO₃ and Fe₂O₃ distribution in the investigated rock samples, a cross plot between CaCO₃ and Fe₂O₃ has been established (Figure 8D). The CaCO₃ and Fe₂O₃ relationship indicates that concentration of calcium carbonate is relatively higher as compared to Fe₂O₃ concentration. Samples enriched in CaCO₃, such as BS-1 (6.78%) and BS-7 (5.72%), contain negligible Fe₂O₃ (0-0.01%), while Fe₂O₃-rich samples, for instance BS-19 (0.19%) and BS-20 (0.21%), are associated with very low CaCO₃ contents (≤2.65%). The cross plot CaCO₃ and Fe₂O₃ illustrates an inverse relationship between the concentrations of

calcium carbonate and iron oxide, indicating that these are not geochemically compatible (Figure 8D). The high concentration of CaCO₃ reflects carbonate rich lithologies with slight iron input, whereas higher Fe₂O₃ in CaCO₃ poor samples points to localized iron enrichment from silicate or oxide phases.

4.1.5 Geochemical Compatibility of BaSO₄ and Fe₂O₃

Detected BaSO₄ values i.e., ranging from 75.4% (BS-1) to 93.45% (BS-11), and Fe₂O₃ values (i.e., 0% to 0.21%) in the representative rock samples exhibit measurable variability. In order to better understand there lative trend of elemental composition in different rock samples, across plot of BaSO₄ versus Fe₂O₃ has been established (Figure 8E). The cross plot demonstrates a strong dominance of barite, while Fe₂O₃ remains extremely low across all samples. In the examined rock samples having higher values, such as BS-19 (0.19%) and BS-20 (0.21%), occur together with constantly high BaSO₄ contents (89.1% and 87.19%, respectively). This distribution shows that BaSO₄ and Fe₂O₃, are geochemically incompatible, where mineralization of barite develops in environments that exclude significant iron enrichment. The verv of Fe₂O₃ suggests concentration minimal contribution from ferromagnesian or iron-bearing silicates, supporting that the mineralization is overwhelmingly barite dominated with very less iron oxide influence.

4.1.6 Geochemical Compatibility of SiO2 and Fe2O3

The SiO₂ vs Fe₂O₃ relationship indicates that both oxides occur normally in low concentrations, though silica shows extensive variation i.e., ranging from 1.11% to 14.55% and Fe₂O₃ ranging from 0% to 0.21% respectively. Most samples with high SiO₂ concentration, such as BS-1 (14.55%) and BS-15 (12.44%), contain very less concentration of Fe₂O₃ (≤0.01%), while the highest Fe₂O₃ enrichments such as BS-19 (0.19%) and BS-20 (0.21%), correspond to moderate silica values (4-7%) as shown in Figure 8F. The cross plot of SiO₂ vs Fe₂O₃ illustrates an inverse relationship between the concentrations of silicon oxide and iron oxide suggesting limited geochemical

compatibility, with silica mostly representing detrital or siliceous input, while Fe₂O₃ reflects minor iron oxides from accessory phases. Their distribution

highlights distinct sources and minimal overlap within the barite mineralization system.



Figure 8. Cross plots of the major composition observed in the analyzed samples exhibiting i.e., BaSO4 vs SiO2 (wt.%), BaSO4 vs CaCO3 (wt.%), CaCO3 vs SiO2 (wt.%), CaCO3 vs Fe2O3 (wt.%), BaSO4 vs Fe2O3 (wt.%), and SiO2 vs Fe2O3 of the barite samples and their corresponding host rock samples. (A) cross plot of BaSO4 vs SiO2 (wt.%) reflects that the concentration of BaSO4 decreases with increasing SiO2 contents in barite samples, representing inverse relationship and geochemically incompatibility of barite and quartz. (B) cross plot of BaSO4 vs CaCO3 (wt.%) reflects that the

concentration of BaSO4 decreases with increasing SiO2 contents and vice versa in the barite samples, reflecting inverse relationship and geochemically incompatibility of barite and quartz. (C) cross plot of SiO2 vs CaCO3 (wt.%) reflects that the concentration of SiO2 increases with increasing CaCO3 contents and vice versa, reflecting direct relationship and geochemically compatibility of calcite and quartz. (D-F) cross plots of CaCO3 vs Fe2O3 (wt.%), BaSO4 vs Fe2O3 (wt.%), and SiO2 vs Fe2O3 of the barite samples and their corresponding host rock samples reflects that the

concentration of CaCO3, BaSO4 and SiO2 increases but due to very low values of Fe2O3 no increase or decrease was observed in the cross plots.

4.2 Oxide-Level Relationships and Trace Compatibility

4.2.1 Geochemical Compatibility of BaO and FeO The compatibility study between BaO and FeO reveals a strong dominance of BaO, with concentrations ranging from ~53% to 67%, while FeO remains negligible across all the representative samples. In some samples e.g., BS-19 and BS-20, FeO shows slight enrichment, BaO values remain relatively high, indicating no positive correlation. Representative samples like BS-3 (BaO = ~67%, FeO \approx 0) and BS-11 (BaO = \sim 63%, FeO \approx 0) confirm that FeO is effectively absent in barite-rich compositions (Figure 9A). This pattern demonstrates that BaO and FeO are not geochemically compatible, reflecting selective mineralization conditions in which barite crystallized independently of ironbearing phases.

4.2.2 Geochemical Compatibility of BaO and K2O

Variable barium oxide values, i.e., ranging from 52.91% (BS-7) to 67.04% (BS-3) and potassium oxide in trace amount (0-1.17%) were detected in the investigated samples. In order to understand the geochemical compatibility of the elemental composition in the analyzed rock samples, across plot between BaO and K2O has been established (Figure 9B). Samples such as BS-3 (BaO = 67.04%, $K_2O = 0$) and BS-11 (BaO = 63.46%, $K_2O = 0.48$) highlight the dominance of BaO with negligible potassium contribution (Figure 9B). The highest K₂O values, observed in BS-19 (1.13%) and BS-20 (1.17%), are accompanied by moderate BaO levels (~56-60%), suggesting that potassium enrichment is unrelated to barite mineralization. Furthermore, it indicates that BaO and K2O are not geochemically compatible, with BaO reflecting barite formation and K2O likely introduced from minor silicate or clay impurities rather than being part of the mineralizing system.

4.2.3 Geochemical Compatibility of BaO and SO₃

The geochemical relationship between BaO and SO₃ shows a strong positive compatibility, reflecting the stoichiometric control of barite (BaSO₄). BaO

concentrations vary between 52.91% (BS-7) and 67.04% (BS-3), while SO₃ ranges from 31.47% (BS-3) to 46.50% (BS-16). Samples enriched in BaO, such as BS-3 (BaO = 67.04%, SO₃ = 31.47%) and BS-11 (BaO = 63.46%, SO₃ = 36.30%), consistently display corresponding SO₃ values that balance the barite composition (Figure 9C). Conversely, higher SO₃ contents, such as in BS-16 (46.50%) and BS-15 (44.70%), are associated with relatively lower BaO values (53.11% and 55.24%). This relationship shows that BaO and SO3 are geochemically compatible, and their coupled variations directly reflect barite mineralization processes. The abovementioned data confirm that the investigated rock samples demonstrate well crystallized barite with variations because of compositional heterogeneity or impurities.

4.2.4 Geochemical Compatibility of BaO and SrO

Variable concentrations of BaO (ranging from 52.9% to 67.04%) and SrO (0.06% to 1.09%) were detected during the geochemical investigation of the representative rock samples (Table 2). In order to understand the probable geochemical relationship between BaO and SrO in various rock samples, a cross plot between BaO and SrO has been established. The BaO concentration is high while the SrO shows very low concentration which reveals a distinct geochemical relationship between these two oxides (Figure 9D). This indicates that Barium is dominant in the investigated sample, confirming Barite (BaSO₄) as the major mineral phase. The less amount of SrO suggests that Strontium shows a limited but significant substitution for Barium int the Barite crystal matrix. This substitution is likely due to the same ionic radii and comparable geochemical behavior of Ba2+ and Sr2+ ions. The BaO and SrO are geochemical incompatibility but shows a positive pattern, suggesting that Sr can replace Ba in the crystal structure, the extent of such replacement remains restricted. These results in the studied rock sample describe that Sr as a trace incorporated element into Barite through isomorphic substitution mechanisms.

4.2.5 Geochemical Compatibility of CaO and SrO

Major and minor oxides detected in the investigated rock samples collected from the study area include variable concentrations of CaO (0-0.37%) and SrO

(0.06-1.09%), respectively (Figure 9E). The CaO vs SrO geochemical compatibility shows a positive trend. The higher CaO concentration of CaO i.e., 0.25-0.37% in samples BS-1 to BS-5 correspond with higher SrO values i.e., 1.0-1.09%, reflecting the geochemical affinity between calcium oxide and strontium oxide due to their same ionic radii and substitution behavior in mineral crystal. On the other hand, very low content of CaO i.e., BS-19 (0.0%) and BS-20 (0.03%) coincide with the lowest SrO values i.e., 0.06% and 0.09%, demonstrate the coupled behavior of these two oxides (Figure 9E). The geochemical compatibility between CaO and SrO in the investigated rock samples of barite is controlled by calcium bearing phases or lattice substitution processes,

4.2.6 Geochemical Compatibility of SrO and FeO

Variable concentration of strontium oxide, and iron oxide were detected in the investigated rock samples (Table 2). The geochemical compatibility between SrO and FeO is weak to moderate negative. The values of SrO range from 0.06% to 1.09%, with relatively higher concentration in BS-2 (1.07%) and BS-4 (1.09%) (Figure 9F). The FeO occurs in trace amounts i.e., 0-0.21%, showing enrichment in rock sample BS-19 (0.19%) and BS-20 (0.21%) where SrO concentration is very low i.e., 0.06% and 0.09%, respectively. The cross plot of these oxides indicates an inverse relationship between the concentrations of strontium oxide and iron oxide. The negative relationship suggests that SrO is in association with barite mineralization due to its geochemical affinity with barium, while iron oxide originates from oxide impurities or minor silicate. This relationship between SrO and FeO suggests that iron oxide does not play a substantial role in the

Strontium bearing mineral phases of the investigated samples.

4.2.7 Geochemical Compatibility of CaO and FeO

Variable calcium oxide values, and iron oxide values were detected in the investigated rock samples (Table 2). The comparison between CaO and FeO shows weak geochemical compatibility (Figure 9G). CaO concentrations are generally low (0-0.37%), with slightly higher values in BS-1 (0.33%) and BS-4 (0.37%), while FeO occurs in minor to trace amounts (0-0.21%). Samples BS-19 (CaO=0.00%, FeO = 0.19%) and BS-20 (CaO = 0.03%, FeO = 0.21%) reveal an inverse relationship, where FeO is relatively enriched despite negligible CaO. This suggests that both oxides are present only as minor impurities, likely sourced from carbonate or silicate phases, and do not exhibit significant geochemical association with barite mineralization.

4.2.8 Geochemical Compatibility of K2O and SrO

Major and minor oxides detected in the investigated rock samples collected from the study area include variable concentrations of K₂O and SrO respectively. The K₂O and SrO geochemical relationship reveals an inverse correlation. Samples having low K2O concentration i.e., 0-0.04%, (BS-1 to BS-5) show concentration of SrO i.e., 1.0-1.09%, demonstrating Strontium enrichment under potassium poor environments. While samples having high content of K2O values (0.39-1.17%) in sample BS-18 to BS-20 shows reduced SrO (0.20-0.09%),highlighting concentration competitive geochemical behavior (Figure 9H). This suggests that Strontium incorporation in barite bearing assemblages is inhibited by increasing potassium activity, because of mineralogical controls or substitution competition in the crystal lattice.

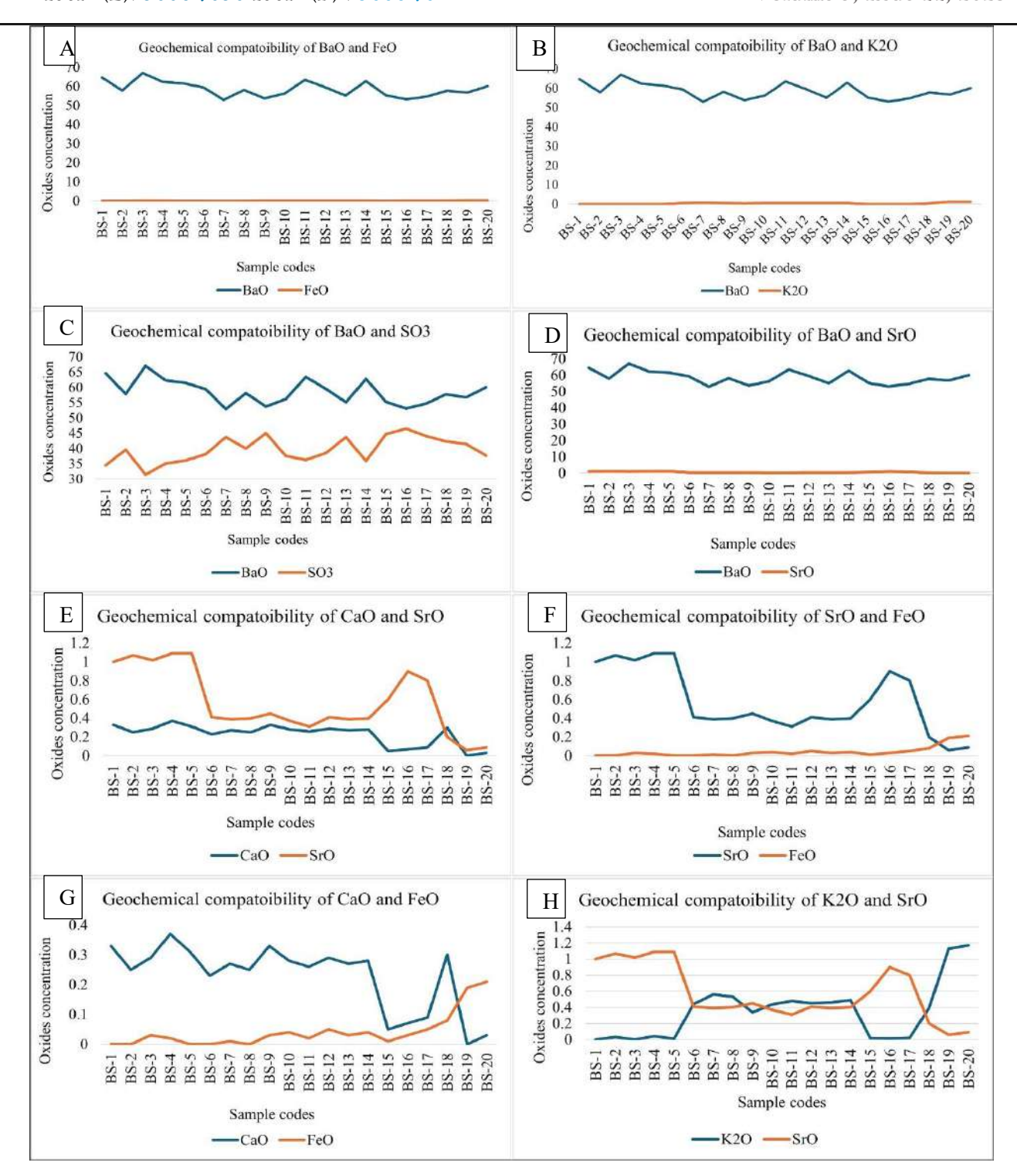


Figure 9. Cross plots of the minor oxides observed in the analyzed samples exhibiting i.e., BaO vs FeO, BaO vs K2O, BaO vs SO3, BaO vs SrO, CaO vs SrO, SrO vs FeO, CaO vs FeO and K2O vs FeO and BaO vs K2O of the barite samples and their

corresponding host rock samples. (A-B) cross plots of BaO vs FeO and BaO vs K2O of the barite samples and their corresponding host rock samples reflects that the concentration of BaO increases but due to very low values of FeO no increase or decrease was

observed in the cross plots. (C) cross plot of BaO vs SO3 reflects that the concentration of BaO decreases with increasing SO3 contents and vice versa in the barite samples, reflecting inverse relationship and geochemically incompatibility of BaO and SO3. (D) cross plots of BaO vs SrO of the barite samples and their corresponding host rock samples reflects that the concentration of BaO increases but due to very low values of SrO no increase or decrease was observed in the cross plots. (E) cross plot of CaO vs SrO reflects that the concentration of CaO decreases with increasing SrO contents and vice versa in the barite samples, reflecting inverse relationship and geochemically incompatibility of CaO and SrO. (F-G) cross plot of SrO vs FeO and CaO vs FeO, a gradual increase of FeO were observed with increasing concentration of CaO and SrO reflecting direct relationship and geochemically compatibility of CaO, FeO and SrO. (H) cross plot of K2O vs SrO reflects that the concentration of K2O decreases with increasing SrO contents and vice versa in the barite samples, reflecting inverse relationship and geochemically incompatibility of K2O and SrO.

5. Discussion and Genetic Implications

The integration of field observation, petrographic studies, and geochemical data provides reliable evidence of hydrothermal barite system and structurally controlled in the Tanawal Formation, shedding light on the hydrothermal processes and tectonic framework responsible for its formation. This study therefore focuses on (1) constraining the timing and source of mineralizing fluids, (2) documenting the paragenetic sequence recorded in the veins, and (3) assessing the economic significance of these high-grade barite occurrences for local supply. Petrographic studies reveal that barite is associated with quartz, biotite, muscovite, and minor sulfides e.g., pyrite, galena, while geochemical data having dominant composition of Ba and SO₄ with minor Sr substitution. Together, these findings suggest late, fault hosted hydrothermal modified by regional deformation. Field observations (Figure 4) demonstrate that barite mineralization in the studied area (Tanawal Formation) occurs predominantly as vein-type bodies filling fractures, joints, and shear planes within quartzose and dolomitic host rocks. The veins, typically 1-5 m thick and extending 10-50 m along strike, exhibit sharp and well-defined contacts with enclosing lithologies. These structural characteristics, along with massive, white to grey barite infill, suggests a hydrothermal vein origin, while mineralizing fluids during late tectonic activity migrated through fault and fracture systems. The presence of cross-cutting relationships with the host rock (Figure 4A) suggests that barite emplacement postdates the main deformation phase of the Tanawal Formation, implying late-stage hydrothermal event.

Petrographic studies reinforce the field evidence (Figures 5-7). Barite appears as coarse-grained, anhedral to subhedral crystals showing high birefringence and perfect cleavage on (001). It is in close association with quartz, biotite, muscovite, and pyrite, forming an interlocking mosaic texture that reflects simultaneous crystallization hydrothermal fluid. The frequent occurrence of quartz-barite intergrowths (Figures 5A-D, 6AB) indicates silica saturation in the fluid, while its association with pyrite (Figures 5CD) suggests reducing conditions during deposition. Trace muscovite and biotite (Figures 6CD, 7A-C) show partial alignment with the schistose host fabric, indicating minor metamorphic overprint related to Himalayan deformation. Geochemical data (Tables 1 and 2) further confirm the hydrothermal origin. The barite samples from the studied are shows high BaSO₄ contents (75.4-94.3 wt.%, avg. ~86-88 wt.%), which indicates remarkably pure mineralization. BaO values (55.24-65.08 wt.%) and SO₃ (36.1-54.5 wt.%) confirm barite as the dominant phase. The inverse relationship between BaSO₄ and SiO₂ (1.56-14.55 wt.%) point out that the investigated samples richest in barite contain the least quartz impurity, consistent with hydrothermal precipitation rather than sedimentary accumulation. Minor CaO and Fe₂O₃ suggest limited inclusion of carbonates and sulfides from host rocks. Trace element patterns also support a hydrothermal setting. SrO contents (0-0.51 wt.%) indicate limited Sr substitution within the barite lattice a typical feature of hydrothermal barite (Hanor, 2000). CuO (up to 0.29 wt.% in BS-5) and ZnO (≤0.19 wt.%) point to minor sulfide mineralization, consistent with field evidence of copper and galena traces along vein margins (Figure

4DE). While the specific gravity values (3.7-4.27) correlate positively with BaSO₄ content, reaffirming high-grade barite purity.

Collectively, the petrographic and geochemical studies show precipitation from hydrothermal fluids rich in Ba and SO₄, migrating along fault-controlled pathways in a reducing environment. The association of these oxides in association with quartz and muscovite suggests that the fluids is in interaction with sedimentary rock i.e., siliciclastic and metamorphic rocks, acquiring silica and alkalis during circulation of these fluids. With minor metamorphic reactivation likely remobilized or resealed existing veins during the later deformation, creating the observed textural variations. Therefore, the complete mineral assemblage, texture, and chemistry support a late-stage tectonic hydrothermal genesis of barite in the Tanawal Formation.

The integrated evidence reveals that barite mineralization in the studied area (Tanawal Formation) is not only structurally controlled but also economically significant. The concentration of BaSO₄ (up to 94 wt.% as shown in Table 2) and low concentration of FeO, CaO, and K₂O indicate a high chemical grade, suitable for use in the oil and gas industry as a weighting agent and in other industries application such as chemical and pigment industries. Although some veins are moderate in size i.e., 1-5 m thick and 10-50 m long, their cumulative tonnage in the studied area (Khanano Dheri) area may represent an important local resource for small to medium scale extraction. In geological point of view, localization of barite along faults and fractures parallel to the Lesser Himalayan structural grain indicates strong tectonic control on fluid migration. The Tanawal Formation, nearby the Mansehra Granite and influenced by Panjal Thrust related deformation, providing an ideal brittle host for hydrothermal circulation. The upward migration of Ba and SO₄ bearing fluids during late orogenic uplift mirrors barite systems in Hazara, Swabi, and the Indian Dharwar Craton, where mineralization follows reactivated faults under compressional transpressional regimes (Deb et al., 1991; Malkani, 2000; Müller et al., 2017).

Hence, the genetic model proposed in this study supports a late tectonic, fault hosted hydrothermal origin, where basinal fluids carrying dissolved barium interacted with sulfate-rich or carbonate horizons, precipitating barite upon cooling and fluid mixing. To understanding the relationship of this tectonic and hydrothermal is critical for targeting mineralized zones within the Tanawal Formation and adjacent terranes. Overall, the integrated data suggest that the barite veins of the Tanawal Formation at Khanano Dheri formed through hydrothermal activity linked to metamorphic deformation. The veins precipitated from Ba and SO₄ bearing fluids circulating along fractures within the quartz-rich metasedimentary rocks. The mineral assemblage such as barite, quartz, biotite, muscovite, and minor pyrite/galena are coupled with high BaSO₄ purity, characterizes epigenetic hydrothermal systems rather than stratiform or SEDEX origins.

From an applied standpoint, the high-grade purity and predictable structural setting make these veins a valuable local resource. However, given their limited lateral continuity, exploration should target structural corridors, particularly fault intersections, dilational zones, and lithological contrasts within the Tanawal Formation. Geophysical and geochemical prospecting could further delineate subsurface extensions and guide resource evaluation. The findings from this study therefore clarify the genetic evolution of barite in the Tanawal Formation and provide a framework for future exploration in similar tectono-metamorphic settings of northern Pakistan.

6. Conclusion

This study reveals that barite mineralization in the Khanano Dheri area of Buner District, Pakistan, formed predominantly through hydrothermal processes associated with faulting and regional tectonism during the Himalayan Orogeny. Field observations show that barite occurs mainly as veins within quartz-rich rocks such as quartzose sandstone and quartzite, indicating structural control and a with silica-bearing link lithologies. Petrographic investigations confirm the presence of barite intergrown with quartz, biotite, muscovite, and minor pyrite, reflecting crystallization from hydrothermal fluids. Geochemical analyses further support this origin, showing high BaSO₄ purity with limited trace element variation and elevated Sr

of characteristic deep-sourced contents, hydrothermal fluids. The regional metamorphism and deformation of the Tanawal Formation likely facilitated fluid migration and mineral precipitation along fault and fracture systems. Altogether, these findings demonstrate that the Khanano Dheri represent structurally controlled, latedeposits tectonic hydrothermal mineralization significant economic potential. Beyond advancing geological understanding, this study provides a foundation for targeted exploration and sustainable utilization of barite resources within northern Pakistan tectono-metamorphic terrains.

REFERENCES

- Abraham, E. I., Bayode, B. L., Olubambi, P. A., Adetunji, A. R., & Onwualu, A. P. (2021). Characterization of barite ores from selected locations in Nigeria for drilling fluid formulation. *Scientific African*, 14, e01057.
- Afolayan, D. O., Adetunji, A. R., Onwualu, A. P., Onwualu, A., Ogolo, O., & Amankwah, R. K. (2021). Characterization of Barite Reserves in Nigeria for Use as Weighting Agent in Drilling Fluid. Journal of Petroleum Exploration and Production Technology, 11(5), 2157-2178. doi:10.1007/s13202-021-01164-8.
- Ahmad M.I., Klinger F.L. 1967. Barite deposits near Khuzdar. Pak-series report 21, GSP-USGS publication.
- Ahmad Z. 1969. Directory of Mineral deposits of Pakistan. GSP, Rec. 15(3): 200p.
- Ahmed, A., Basfar, S., Elkatatny, S., & Bageri, B. (2022). Vermiculite for enhancement of barite stability in water-based mud at elevated temperature. *Powder Technology*, 401, 117277.
- Ahsan, S. N., & Khan, K. S. A. (1994). Pakistan mineral prospects: lead and zinc. In Int. round table conf. on Foreign investment in Exploration and mining in Pakistan, Ministry of Petroleum and Natural resources, Islamabad, 10b.
- Ahsan, S. N., & Mallick, K. A. (1999). Geology and genesis of barite deposits of Lasbela and Khuzdar Districts, Balochistan, Pakistan. *Resource Geology*, 49(2), 105-111.

- Ali, K., Ghaffar, A., Ullah, I., Murad, F., Ahmed, J., & Baloch, M. I. (2021). Geology, Petrography, and Mineralization of Sedimentary Hosted Strata-Bounded Barite Deposit at Gunga, Khuzdar District Balochistan, Pakistan. International Journal of Economic and Environmental Geology, 12(4), 43-50.
- Bonel, K. A. (2005). Barytes.
- Calkins, J. A., Jamiluddin, S., Bhuyan, K., & Hussain, A. (1981). Geology and mineral resources of the Chitral-Partsan area, Hindu Kush Range, northern Pakistan (No. 716-G). US Govt. Print. Off.; for sale by the Distribution Branch, US Geological Service.
- Ciullo, P. A. (1996). Industrial minerals and their uses: a handbook and formulary. William Andrew.
- Deb, M., & Goodfellow, W. D. (2004). Sediment Hosted Lead-Zinc Sulphide Deposits. CRC Press. Narosa Publication House, New Delhi, Australia and Canada, p. 367.
- Deb, M., Hoefs, J., & Bauman, A. (1991). Isotopic composition of two Precambrian stratiform barite deposits from the Indian shield. *Geochimica* et Cosmochimica Acta, 55(1), 303-308.
- Deb, M., & Pal, T. (2015). Mineral potential of Proterozoic intracratonic basins in India. Geological Society, London, Memoirs 43 (1), 309–325. https://doi.org/10.1144/M43.21.
- Hanor, J. S. (2000). Barite celestine geochemistry and environments of formation. *Reviews in Mineralogy and Geochemistry*, 40(1), 193–275. https://doi.org/10.2138/rmg.2000.40.4
- Hussain, H. M., Al-Haidarey, M., Al-Ansari, N., and Knutsson, S. (2014). Evaluation and mapping groundwater suitability for irrigation using GIS in Najaf governorate, IRAQ. J. Environ. hydrology 22.
- Joyce Griffrths, Industrial Minerals, No.246, March (1988)
- Klinger F.L., Abbas S.H. 1963. Barite deposits of Pakistan. CENTO Symp. Indust. Rocks and Min. Lahore, 418-428.

- Klinger, F. L., & Abbas, S. H. (1962). Barite deposits of Pakistan. In CENTO Symposium on Industrial Rocks and Minerals (pp. 418-428).
- Klinger, F. L., & Richards, R. L. (1973). Barite in *Pakistan* (No. 73-145). US Geological Survey],.
- Kontak, D. J., Kyser, K., Gize, A., & Marshall, D. (2006). Structurally controlled vein barite mineralization in the Maritimes Basin of eastern Canada: Geologic setting, stable isotopes, and fluid inclusions. *Economic Geology*, 101(2), 407-430.
- Dora, M. L., Roy, S. K., Khan, M., Randive, K., Kanungo, D. R., Barik, R., ... & Mayachar, G. K. (2022). Rift-induced structurally controlled hydrothermal barite veins in 1.6 Ga granite, Western Bastar Craton, Central India: Constraints from fluid inclusions, REE geochemistry, sulfur and strontium isotopes studies. *Ore Geology Reviews*, 148, 105050.
- Malkani M.S. (2000). Preliminary report on gypsum deposits of Sulaiman Range, Pak. GSP, IR (706): 1-11.
- Malkani M.S. (2010b). New Pakisaurus (Pakisauridae, Titanosauria, Sauropoda) remains, and Cretaceous Tertiary (K-T) boundary from Pakistan. Sindh University Research Journal (Science Series). 42 (1), 39-64.
- Malkani M.S., Tariq M. (2000). Barite Mineralization in Mekhtar area, Loralai District, Balochistan, Pakistan, GSP IR 672, 1-9.
- Malkani M.S., Tariq M. (2004). Discovery of barite deposits from the Mekhtar area, Loralai District, Balochistan, Pakistan. In abstract volume National Conference on Economic and Environmental sustainability of Mineral resources of Pakistan, Baragali, Pakistan, 48.
- Malkani, M. S., & Mahmood, Z. (2017). Mineral Resources of Pakistan: provinces and basins wise. Geological Survey of Pakistan, Memoir, 25, 1-179.

- Margoum, D., Bouabdellah, M., Klügel, A., Banks, D.A., Castorina, F., Cuney, M., J´ ebrak, M., Bozkaya, G., (2015). Pangea rifting and onward pre-central Atlantic opening as the main ore-forming processes for the genesis of the Aouli REE-rich f luorite-barite vein system, Upper Moulouya District. Morocco. J. Afr. Ear. Sci. 108, 22–39. https://doi.org/10.1016/j.jafrearsci.2015.03.021.
- Monnin, C., Cividini, D., (2006). The saturation state of the world's ocean with respect to (Ba, Sr) SO4 solid solutions. Geochim. Cosmochim. Acta 70, 3290–3298. https://doi.org/10.1016/j.gca.2006.04.002.
- Muller, A., Ehle, H., (2021). Rapid ore classification for real-time mineral processing optimization at the Niederschlag multi-generation hydrothermal barite-fluorite vein deposit, Germany. Miner. Deposita 56, 417–424. https://doi.org/10.1007/s00126-020-01037-w.
- Muller, E., Philippot, P., Rollion-Bard, C., Cartigny, P., Assayag, N., Marin-Carbonne, J., Mohan, R., Sarma, S., (2017). Primary sulfur isotope signatures preserved in high-grade Archean barite deposits of the Sargur Group, Dharwar Craton. India. Precam. Res. 295, 38–47.
 - https://doi.org/10.1016/j.precamres.2017.0 4.029.
- Nadoll, P., So´snicka, M., Kraemer, D., Duschl, F., (2019). Post-Variscan structurally- controlled hydrothermal Zn-Fe-Pb sulfide and F-Ba mineralization in deep-seated Paleozoic units of the North German Basin: A review. Ore Geol. Revs. 106, 273–299. https://doi.org/10.1016/j.oregeorev.2019.0 1.022.
- Neelakantam, S. (1987). Mangampet barites deposit, Cuddapah District, Andhra Pradesh. Radhakrishna, B. P. (ed.) Purana Basins of Peninsular India. Geol. Soc. India, Bangalore, Memoirs. 6. 429–458.

- Okubo, J., Klyukin, Y.I., Warren, V.L., Sublett Jr., D.M., Bodnar, R.J., Gill, B.C., Xiao, S., (2020). Hydrothermal influence on barite precipitates in the basal Ediacaran Sete Lagoas cap dolostone, Sao Francisco Craton, central Brazil. Precam. Res. 340, 105628 https://doi.org/10.1016/j.precamres.2020.105628.
- Radhakrishna, B.P., Vaidyanadhan, R. (1997).

 Geology of Karnataka; Published by the Geol. Soc. India, Bangalore.DOI: https://doi.org/10.1180/minmag.1998.062.
 6.03.
- Robinson Jr, G. R., & Woodruff, L. G. (1988). Characteristics of base-metal and barite vein deposits associated with rift basins, with examples from some early Mesozoic basins of eastern North America. US Geological Survey, Bulletin, 1776, 377-390.
- Samaoui, S., Aabi, A., Nguidi, M. A., Boushaba, A., Belkasmi, M., Baidder, L., ... & Zehni, A. (2023). Fault-controlled barite veins of the eastern Anti-Atlas (Ougnat, Morocco), a farfield effect of the Central Atlantic opening? Structural analysis and metallogenic implications. *Journal of African Earth Sciences*, 204, 104970.
- Staude, S., Gob, S., Pfaff, K., Strobele, F., Premo, W.R., Markl, G., (2011). Deciphering fluid sources of hydrothermal systems: a combined Sr- and S-isotope study on Barite (Schwarzwald, SW Germany). Chem. Geol. 286, 1–20. https://doi.org/10.1016/j.chemgeo.2011.04.009.

- U.S. Geological Survey (USGS) (2017) Critical mineral resources of the United States, Barite: mineral commodity summaries, professional paper 1802, U.S. Geological Survey, Reston, VA, pp 30–31. ISBM: 978-1-4113-3991-
 - 0. https://doi.org/10.3133/pp1802A
- U.S. Geological Survey (USGS) (2019) Barite: mineral commodity summaries, prepared by Michele E. McRae, U.S. Geological Survey, VA, pp 28–19
- Walter, B.F., Jensen, J.L., Coutinho, P., Laurent, O., Markl, G., Steele-MacInnis, M., (2020). Formation of hydrothermal fluorite-hematite veins by mixing of continental basement brine and red bed-derived fluid: Schwarzwald mining district. SW Germany. Jour of Geochem. Expl. 212, 106512.
- Walter, B.F., Kortenbruck, P., Scharrer, M., Zeitvogel, C., W"alle, M., Mertz-Kraus, M., G., (2019). Chemical evolution of oreforming brines-Basement leaching, metal provenance, and the redox link between barren and ore-bearing hydrothermal veins.

 A case study from the Schwarzwald mining district in SW-Germany. Chem. Geol. 506,
 - https://doi.org/10.1016/j.chemgeo.2018.12 .038.
- Williams Jones, A.E., Samson, I.M., Olivo, G.R., (2000). The genesis of hydrothermal f luorite-REE deposits in the Gallinas Mountains, New Mexico. Econ. Geol. 95, 327–342.
 - https://doi.org/10.2113/gsecongeo.95.2.32 7.
- Zou, H., Li, M., Santosh, M., Zheng, D., Cao, H.-w., Jiang, X.-W., Chen, H.-F., Li, Z.-Q., (2021). Fault-controlled carbonate-hosted barite-fluorite mineral systems: The Shuanghe deposit, Yangtze Block, South China. Gondwana Res. 101, 26–43. https://doi.org/10.1016/j.gr.2021.07.020.